FULL ARTICLE

Localization of PD-L1 on single cancer cells by iSERS microscopy with Au/Au core/satellite nanoparticles

Elzbieta Stepula[1] | Matthias König[1] | Xin-Ping Wang[1] | Janina Levermann[2] |
Tobias Schimming[3] | Sabine Kasimir-Bauer[2] | Bastian Schilling[3,4] |
Sebastian Schlücker[1]*

[1]Department of Chemistry and Center for
Nanointegration Duisburg-Essen (CENIDE),
University of Duisburg-Essen, Essen,
Germany

[2]Department of Gynecology and Obstetrics,
University Hospital Essen, University of
Duisburg-Essen, Essen, Germany

[3]Department of Dermatology, University
Hospital, University of Duisburg-Essen,
Essen, Germany

[4]Department of Dermatology, University
Hospital in Würzburg, Würzburg, Germany

*Correspondence
Sebastian Schlücker, Department of
Chemistry and Center for Nanointegration
Duisburg-Essen (CENIDE), University of
Duisburg-Essen, Universitätsstr. 5, Essen
45141, Germany.
Email: sebastian.schluecker@uni-due.de

Abstract
Programmed cell death-ligand 1 (PD-L1) is
an important predictive biomarker. The
detection of PD-L1 can be crucial for patients
with advanced cancer where the use of
immunotherapy is considered. Here, we dem-
onstrate the use of immuno-SERS micros-
copy (iSERS) for localizing PD-L1 on single
cancer SkBr-3 cells. A central advantage of
iSERS is that the disturbing autofluorescence
from cells and tissues can be efficiently
minimized by red to near-infrared laser excitation. In this study we employed
Au/Au core/satellite nanoparticles as SERS nanotags because of their remarkable
signal brightness and colloidal stability upon red laser excitation. False-color iSERS
images of the positive and negative controls clearly reveal the specific localization
of PD-L1 with SERS nanotag-labeled antibodies.

KEYWORDS
gold nanoparticles, PD-L1, Raman, SERS
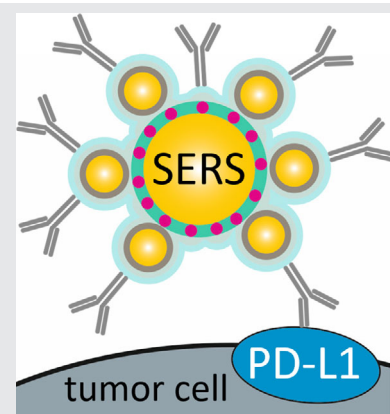
1 | INTRODUCTION

Programmed cell death-ligand 1 (PD-L1) plays a crucial role
in immune regulation and is expressed in numerous healthy
tissues, for example, in the placenta [1]. PD-L1 also mediates
immune evasion in many solid and hematological malignan-
cies including malignant melanoma and breast cancer [2–4].
Blockade of programmed cell death-1 (PD-1) and its ligand
PD-L1 is used as an immunotherapy employing so called
immune checkpoint inhibitors (ICI). ICI has been shown to
prolong progression-free (PFS) and overall survival (OS) in
different cancers and has become a common denominator in

modern oncology [5–7]. This impressive and wide clinical
activity can be accompanied by severe immune-related
adverse events (irAE) and although rare, treatment-related
deaths [8, 9]. In addition, maximum benefit might be
restricted to patients with certain characteristics [10] and
detection of biomarkers including but not limited to T cell
infiltration, mutational load and PD-L1 expression [11–13].
Very recently, a prospective, randomized phase 3 trial in
advanced untreated triple-negative breast cancer (TNBC)
showed increased PFS in patients receiving the PD-L1 block-
ing antibody atezolizumab plus nab-paclitaxel in comparison
to nab-paclitaxel plus placebo [14]. Increased OS by adding

atezolizumab to nab-paclitaxel was only reported for PD-L1 positive tumors. Methods and assays for detecting biomarkers are therefore key to use ICI with maximum clinical benefit.

Nowadays immunohistochemistry (IHC) remains the gold standard for localizing PD-L1 on cancerous tissue. However, the evaluation of IHC slides from, for example, skin cancer patients is very difficult even for experienced pathologists for reasons listed below [11]. Melanoma develops from melanocytes cells, with a color which is similar to that of the product of the HRP enzyme reaction. Immunofluorescent staining is not really an attractive alternative to IHC due to the very strong autofluorescence of the sample caused by the brown pigment [15].

A promising alternative to IHC and IF is immuno-SERS microscopy (iSERS) [16]. This emerging technique is based on surface-enhanced Raman scattering (SERS) for optical readout and circumnavigates the problems associated with IHC and IF [17, 18]. In iSERS antigens are localized via target recognition by antibodies as in other immuno-based methods. However, instead of labeling the antibody with an enzyme or a fluorophore, a molecularly functionalized noble metallic nanoparticle is employed [19]. In our work we used Au/Au core/satellite particles with Raman-active reporter molecules on the surface [20]. The unique Raman signature of the molecule can be enhanced by the gold nanostructure upon resonant optical excitation and is used for the identification of the particles [21]. The SERS nanotag-antibody conjugates are then localized on single cells or tissue specimen by Raman microspectroscopy. With the help of iSERS it is possible to overcome the limitations of the standard techniques for localizing PD-L1 on skin tissue since the use of SERS nanotags instead of HRP enzyme or fluorophores has several advantages. As mentioned before, specimens with malignant melanoma exhibit strong autofluorescence. This can be overcome by the application of red to near-infrared laser excitation which minimizes the disturbing effect of autofluorescence and improves the image contrast [22, 23]. In contrast to fluorescent dyes, the nanotags are chemically stable and inert against photobleaching. Overall, iSERS is a fast and reproducible method for protein localization on single cancer cells [24, 25].

2 | MATERIALS AND METHODS/ EXPERIMENTAL

2.1 | Materials

Tetrachloroauric acid (HAuCl$_4$ • 3 H$_2$O), 1-ethyl-3-(3-dimethylaminopropyl)carbodiimide (EDC), *N*-hydroxysulfosuccinimide sodium salt (sulfo-NHS), bovine serum albumin (BSA), (11-mercaptoundecyl)-*N,N,N*-trimethylammonium bromide (MUTAB), poly(sodium-4-styrenesulfonate) (PSS), 7-mercapto-4-methylcoumarin (MMC) and 4-(2-hydroxyethyl)-1-piperazine ethane sulfonic

acid (HEPES) were purchased from Sigma Aldrich. Phosphate buffered saline (PBS) was prepared by dissolving powder purchased from Biochrom GmbH, Germany, in Milli-Q water. Paraformaldehyde (PFA) solution (4% in PBS) was obtained from Affymetrix/Thermo Fisher, Germany. Rabbit anti-PD-L1 antibody [clone 28-8] was obtained from Abcam, Germany. Goat anti-rabbit antibody was purchased from Thermo Fisher, Germany. Ultrapure water (18.2 MΩ cm, Millipore) was used throughout the experiments.

2.2 | Cell culture and preparation

The human breast cancer cell line SkBr–3 was purchased from American Type Culture Collection (ATCC, Manassas, Virginia). SkBr–3 cells were cultured in McCoy's 5a Medium (Gibco by Life Technologies, Thermo Fisher Scientifc, Waltham, Massachusetts) supplemented with 10% (vol/vol) fetal calf serum (Gibco), 1% (vol/vol) penicillin-streptomycin (Sigma Aldrich, St. Louis, Missouri), 7.5% (vol/vol) sodium bicarbonate (Gibco) and 200 mM L-glutamine (Gibco). Cells were grown at 37°C in a humidified atmosphere with 5% CO$_2$. Subcultivation was performed with trypsin-EDTA solution (0.05% trypsin, 0.02% EDTA, Sigma Aldrich). A total number of ca. 10^5 SkBr3 cells were cytospinned on glass slides coated with poly-L-lysine (R. Langenbrinck, Emmendingen, Germany) at 1000 g for 6 minutes and air-dried overnight at RT.

2.3 | Synthesis of SERS nanotags and antibody conjugates

The Au/Au core/satellite nanoparticles comprise a positively charged 50 nm gold nanosphere (core) [26, 27] with a smooth surface (AuNSs), coated with the linker molecule MUTAB and the Raman reporter MMC, as well as negatively charged 30 nm gold nanoparticles (satellites) (AuNP) [28]. The assemblies are stabilized by a PEG shell (HS-PEG-COOH) to avoid non–specific binding of the SERS nanotags to cells. The last step is the bioconjugation of antibodies to the SERS nanotags. The carboxyl groups were activated by EDC/sulfo-NHS for 25 minutes at RT. The rabbit anti-PD-L1 antibody was added to the activated SERS colloid and incubated for 2 hours at RT and then overnight at 4°C. The suspension was washed with 2% BSA/PBS four times in order to remove any unreacted antibodies and then suspended in 2% BSA/PBS solution for subsequent cell staining.

2.4 | Cell fixation, blocking and staining

The cytospinned cell slides were washed with PBS buffer three times to remove the remaining culture medium. Next, 4% PFA was added onto the cell slides and incubated for 15 minutes at RT for fixation. After incubation, the cell slides were washed

with PBS buffer three times to remove an excess of 4% PFA. In order to unmask the antigen, heat-induced epitope retrieval was performed. The cell slides were heated at 95°C for 10 minutes in citrate buffer pH 6, cooled down and washed in PBS buffer. Then 2% BSA/PBS solution was added to the cells slides as a blocking reagent for 2 hours at RT to reduce any unspecific binding and background. The primary antibody was incubated on the SkBr–3 cell slides for 1 hour at 37°C. Afterward, the slides were stained with the SERS-labeled secondary antibody for 8 hours under shaking. Finally, the cell slides were washed three times with PBS buffer and once with water to remove any unbound SERS nanotags and then mounted.

For the IF staining the primary antibody was incubated on the SkBr–3 cell slides for 1 hour at 37°C. Then, the fluorescent-labeled (AF647 dye) secondary goat anti-rabbit antibody was incubated for 40 minutes at RT. Finally, the cell slides were washed three times with PBS buffer and once with water before mounting.

## 2.5 | iSERS microscopy on single breast cancer cells

Single cells were identified in the bright field for imaging of selected areas by confocal Raman microscopy (WITec alpha 300 R, grating monochromator with $f = 30$ cm focal length, EM-CCD grating). A 40× air objective with cover glass

correction and a NA of 0.6 (Olympus LUC Plan FLN) was used. The 632.8 nm radiation from a He-Ne laser with a power of 1.2 mW at the sample was employed for exciting Raman scattering. The integration time per pixel was 100 ms. For the localization of PD-L1 on single cells, the cells were at first identified in the bright-field. Next an area was selected for the SERS mapping and investigated with an integration time of 100 ms and a laser power of 1.2 mW at the sample. After performing the mapping experiments the recorded SERS spectra were processed. Raw spectra were smoothed via the Savitzky-Golay algorithm (7th order polynomial, 31 points). Then a baseline correction (Whittaker-Henderson procedure [29]) was performed. Mean spectra with error bars were calculated using a MATLAB algorithm (shadedErrorBars). For each pixel the maximum intensity of the Raman peak centered at ca. 1590 cm^{-1} was determined by using a Lorentzian line profile and a nonlinear least square algorithm in order to generate the corresponding SERS false-color images.

3 | RESULTS AND DISCUSSION

3.1 | Characterization of Au/Au core/satellite particles (SERS nanotags)

Figure 1A shows a transmission electron microscopy (TEM) image of a single Au/Au core/satellite particle and Figure 1B
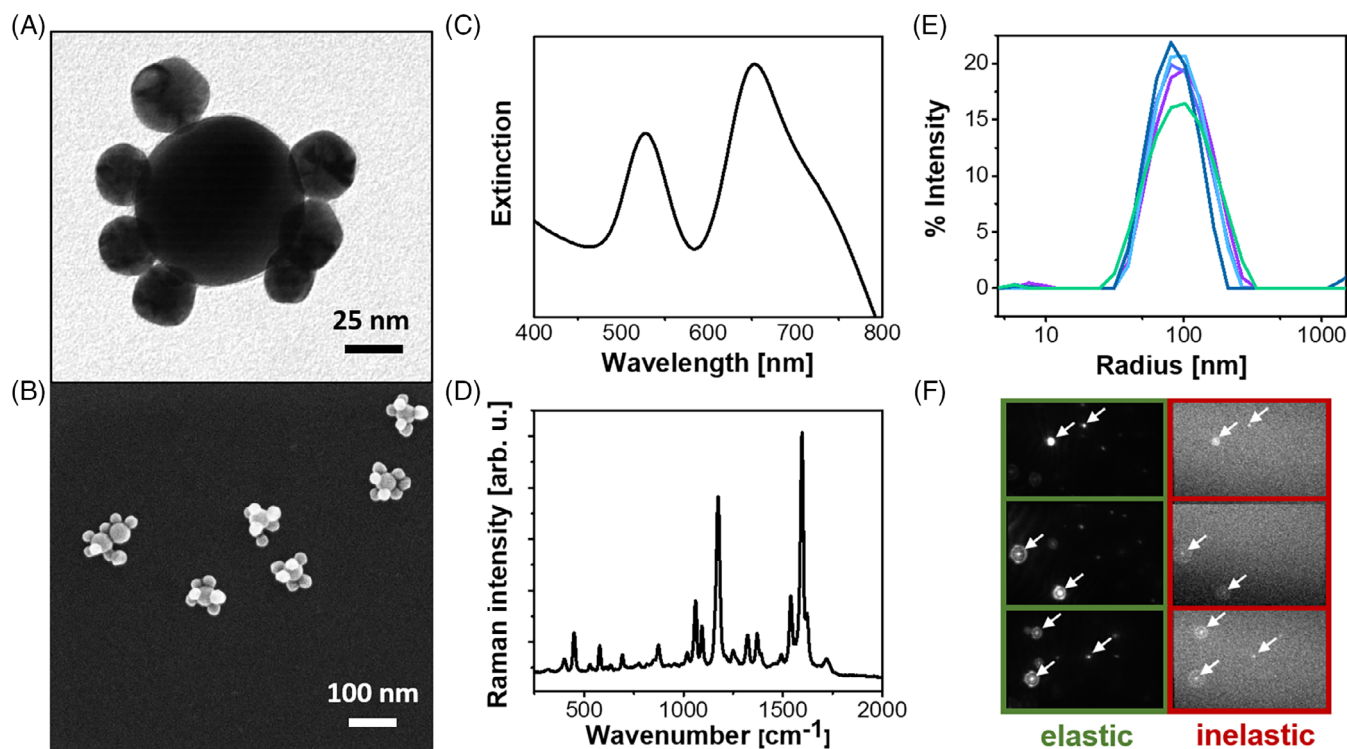
FIGURE 1 Characterization of Au/Au core/satellite particles. A, TEM image; B, SEM image; C, extinction spectrum; D, SERS spectrum of MMC; E, size distribution; F, correlative single-particle real-time imaging. MMC, 7-mercapto-4-methylcoumarin; SEM, scanning electron microscopy; SERS, surface-enhanced Raman scattering; TEM, transmission electron microscopy
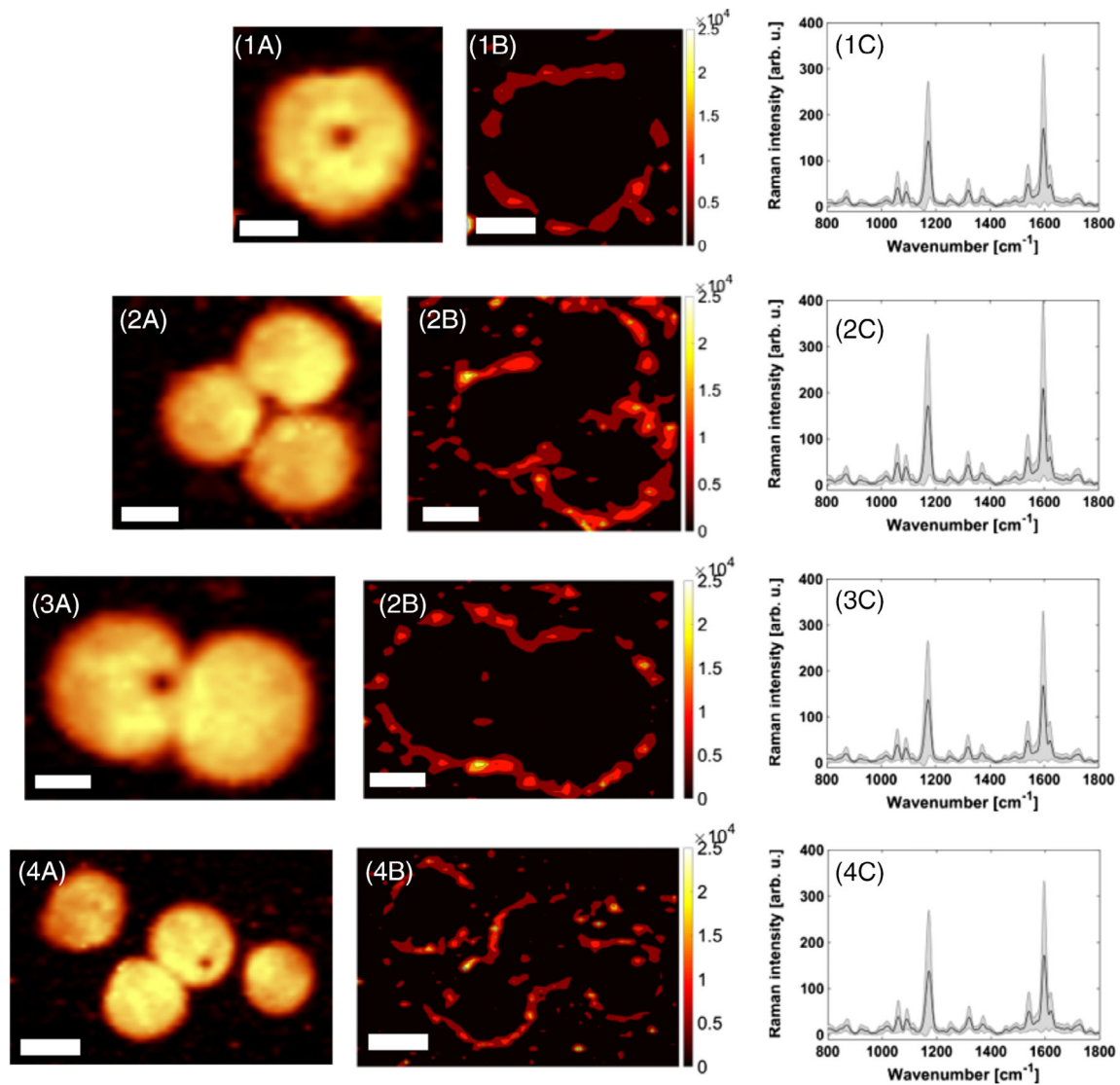
FIGURE 2 Localization of PD-L1 on SkBr-3 cells by iSERS microscopy. Fluorescence images (1A, 2A, 3A, 4A), iSERS false-color images (1B, 2B, 3B, 4B) and mean SERS spectrum (1C, 2B, 3B, 4B). Scale bar is 5 μm. iSERS, immuno-SERS microscopy; SERS, surface-enhanced Raman scattering

a scanning electron microscopy (SEM) image. The UV/Vis extinction spectrum of Au/Au core/satellite particles exhibits two plasmon peaks. The peak at ca. 700 nm is assigned to a plasmon coupling mode of the core and the satellites [30, 31]. A SERS spectrum with the characteristic Raman peak of MMC at 1590 and 1200 cm^{-1} is shown in Figure 1D. Based on DFT calculations, we assign these two normal modes to a C≡C stretching mode and a ring breathing mode, both with dominant contributions from the phenyl ring with the thiol group. The hydrodynamic radius of the particles before the bioconjugation, as determined by dynamic light scattering, is (88 ± 2) nm. Correlative Rayleigh/Raman single-particle real-time imaging of the Au/Au core/satellite particles using a home-built optical setup was performed for demonstrating their single-particle brightness

[32]. Figure 1F shows snapshots from a video recorded during the measurement. Individual particles can be observed in both the elastic (left) and the inelastic (right) channel which confirms the SERS activity of Au/Au core/satellite particles at the single-particle level [28, 33].

3.2 | Specificity of anti-PD-L1-antibody/SERS nanotag-conjugates in single cell iSERS microscopy

The most important aspect in immunostaining is the unambiguous demonstration of binding specificity. This is especially crucial in iSERS microscopy since the relatively large SERS nanotags (~100 nm compared to ca. 15 nm for an
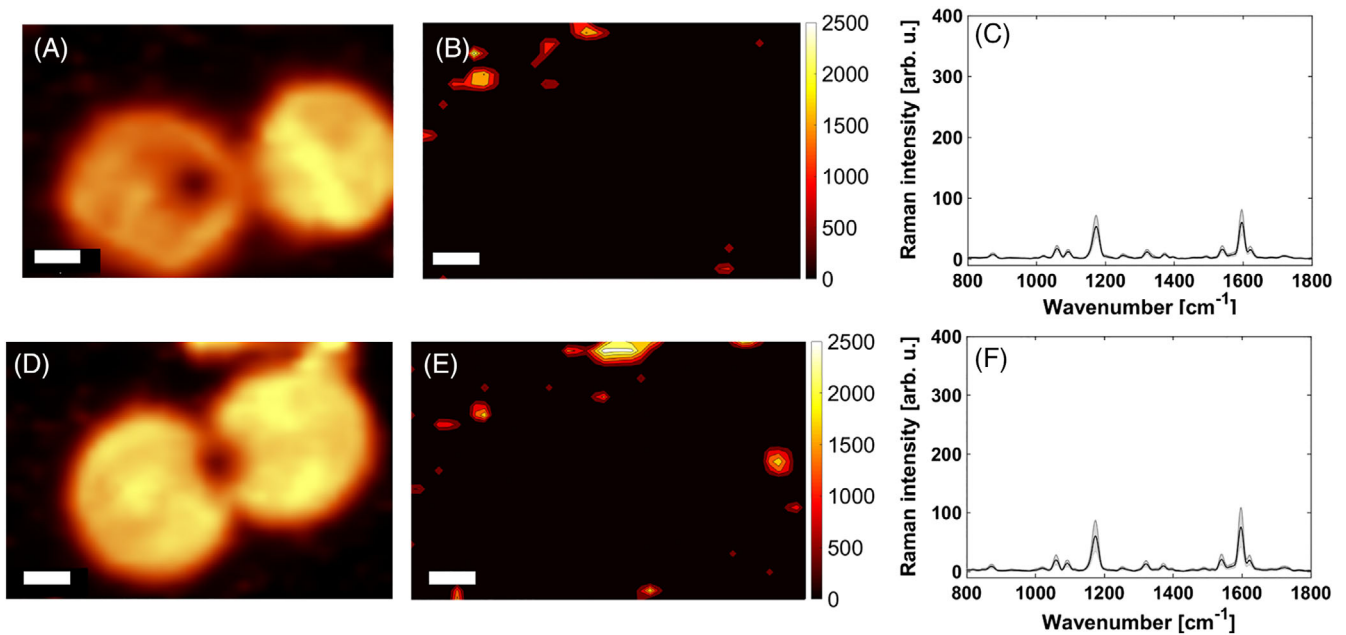
FIGURE 3 Visualization of the contributing low-intensity pixels. A, D, Fluorescence images; B, E, false-color images with reduced color scale bar; and C, F, mean SERS spectrum. Scale bar is 5 μm. SERS, surface-enhanced Raman scattering

FIGURE 4 Four fluorescence images from two different samples (left column: sample 1 and right column: sample 2) with a green filter (1A and 2A) and with a red filter (1B and 2B). Sample 1 (left column) was incubated with both primary AB and the AF647-labeled secondary AB. Sample 2 (right column) is a negative control and was incubated only with the AF647-labeled secondary AB, but not with primary AB. The comparison of image 1B and 2B demonstrates specific binding of the primary anti-PD-L1 AB. The comparison of image 1A and 2A shows the autofluorescence upon excitation with a Hg lamp in combination with a 488 nm excitation filter. AB, antibody
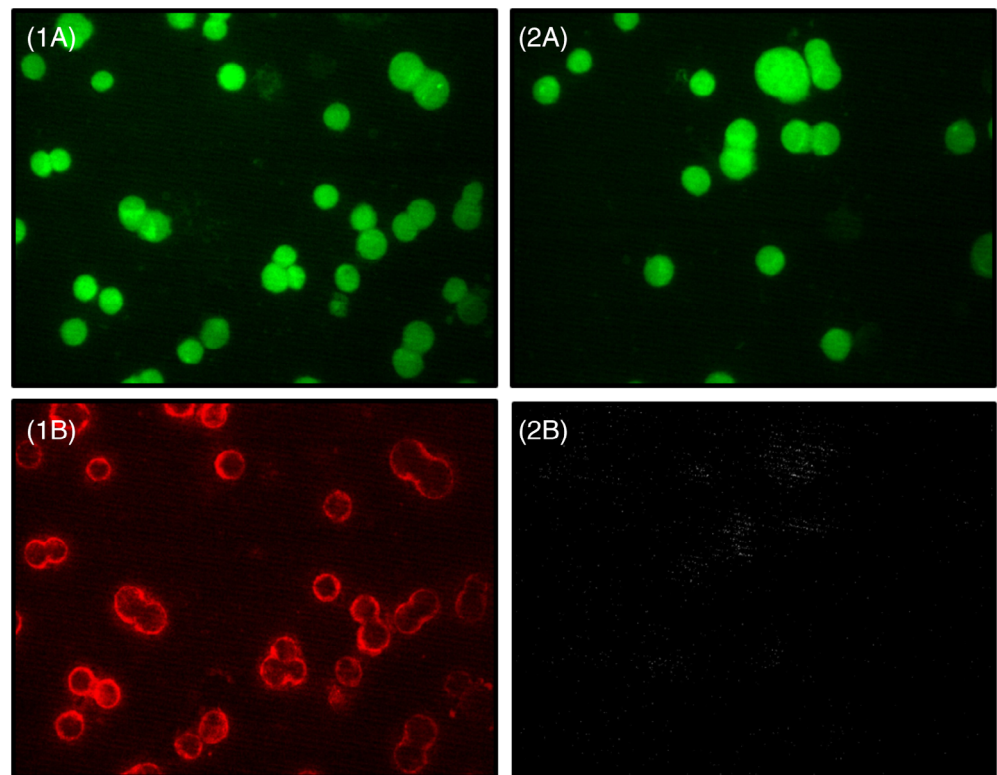
IgG) may affect the binding affinity of the corresponding antibody.

Figure 2 shows the SERS mapping results for four single cells. The exact position of the cell is showed by the fluorescence visualization on the left side (Figures 1A, 2A, 3A and 4A). In the middle the scaled false-color images are shown

(Figures 1B, 2B, 3B and 4B), on the right side the corresponding mean SERS spectra with error bars showing the signal fluctuations (Figures 1C, 2C, 3C and 4C). Yellow and red pixels in the false-color images indicate that the signals of the SERS nanotags were detected. For the interpretation of the false-color SERS images only pixels with

integrated Raman intensities larger than 100 counts (threshold manually set by user) were considered and the color scale was adjusted accordingly. The pattern of the false-color SERS images shows that PD-L1 can be selectively localized on the cell membrane of the SkBr-3 cells.

Negative control experiments were performed in order to confirm the specificity of the staining. Specifically, SERS-labeled secondary antibodies were incubated on SkBr-3 cells without the previous addition of the primary antibody. Positive and negative controls were carried out under the same conditions. The corresponding false-color images are depicted with the same color scale bar. The negative control (Figure S1A,C) shows no pixels with SERS signals above the threshold of 100 counts for the integrated Raman intensity. This suggests that no non–specific binding occurs at all. However, this is certainly not the case. The inspection of the corresponding mean SERS spectrum clearly reveals some detectable signals (Figure S1B,D).

The selective visualization of the contributing low-intensity pixels requires an adjustment of the color scale bar; upon reduction of the upper limit from 25 000 counts (Figure S1A,C) to 2500 counts (Figure 3B,E) the low-intensity pixels attributed to nonspecific binding become visible. In order to assess whether this non-specific binding occur on the cells or on the glass slide, a visualization of the cells is required. We employed the integrated intensity from 300 to 2700 cm^{-1} which covers both SERS and especially also the underlying broad autofluorescence contribution from cellular chromophores. The corresponding image is depicted in Figure 3A,D. A comparison with Figure 3B,E suggests that non-specific binding occurs dominantly on the glass substrate as the low-intensity SERS pixels are mostly observed at positions where no cells are present.

In addition to iSERS experiments also immunofluorescence (IF) staining of the SkBr-3 cells was performed. IF staining of PD-L1 [34] was carried out parallel to the iSERS staining experiments under the same conditions. The only difference is the incubation time with the fluorophore-labeled secondary antibody (40 minutes for IF vs 8 hours for iSERS). We suppose that the reason for the longer incubation time for iSERS might be the overall size and weight of the SERS nanotags, causing slower binding to the primary antibodies. The fluorescence images are shown in Figure 4.

Overall, the presented false-color images in Figure 2 demonstrate the capability of iSERS for selectively localizing PD-L1 on single SkBr-3 cells. The presented results confirm earlier iSERS PD-L1 results on MDA-MB-231 cells [16].

Stable and bright molecularly functionalized gold nanoparticles (SERS nanotags) with a localized surface plasmon resonance (LSPR) in the red to near-infrared are a pre-requisite for obtaining high quality background-free staining of target proteins such as PD-L1 on colored and autofluorescent specimen. These optical considerations for background-free imaging guide the rational design of SERS nanotags for iSERS microscopy on cells and tissue specimen. Au/Au core/satellite particles fulfill all necessary criteria: (a) they exhibit a LSPR in the red region of the UV/Vis extinction spectrum; (b) they are bright since plasmonic coupling between the Au core and the Au satellites leads to hot spots (very high local electric field strengths), which generate very strong SERS signals; (c) they are stable due to surface chemistry preventing the aggregation of the colloid [33]. We employ Au/Au core/satellite particles with Raman-active reporter molecules on the surface of the core [28]. The unique Raman spectrum of the reporter molecule is enhanced by the gold nanostructure upon resonant optical excitation and is used for the identification of the SERS nanotag [19]. In this proof of concept study we demonstrate the suitability of anti-PD-L1 antibody-Au/Au/ core/satellite nanotag conjugates in iSERS microscopy for the selective localization of the predictive PD-L1 marker on single SkBr-3 cancer cells using SERS nanotags in combination with red laser excitation for minimizing interferences from background and autofluorescence. The negative control experiment with the omission of the primary anti-PD-L1 antibody confirms the binding specificity of the SERS-labeled antibodies. Overall, these promising results on single cells pave the way for future high-quality background-free staining of PD-L1 on tissue specimen. Future work will aim at the localization of PD-L1 on FFPE tissue [35].

ORCID

Sebastian Schlücker https://orcid.org/0000-0003-4790-4616

REFERENCES

[1] M. E. Keir, M. J. Butte, G. J. Freeman, A. H. Sharpe, *Annu. Rev. Immunol.* **2008**, *26*, 677.

[2] S. Ostrand-Rosenberg, L. A. Horn, S. T. Haile, *J. Immunol.* **2014**, *193*, 8.

[3] H. Dong, S. E. Strome, D. R. Salomao, H. Tamura, F. Hirano, D. B. Flies, P. C. Roche, J. Lu, G. Zhu, K. Tamada, V. A. Lennon, E. Celis, L. Chen, *Nat. Med.* **2002**, *8*, 8.

[4] H. Ghebeh, S. Mohammed, A. Al-Omair, A. Qattan, C. Lehe, G. Al-Qudaihi, N. Elkum, M. Alshabanah, S. Bin Amer, A. Tulbah, D. Ajarim, T. Al-Tweigeri, S. Dermime, *Neoplasia* **2006**, *8*, 3.

[5] S. L. Topalian, C. G. Drake, D. M. Pardoll, *Cancer cell* **2015**, *27*, 450.

[6] F. S. Hodi, S. J. O'Day, D. F. McDermott, R. W. Weber, J. A. Sosman, J. B. Haanen, R. Gonzalez, C. Robert, D. Schadendorf, J. C. Hassel, W. Akerley, A. J. van den Eertwegh, J. Lutzky, P. Lorigan, J. M. Vaubel, G. P. Linette, D. Hogg, C. H. Ottensmeier, C. Lebbe, C. Peschel, I. Quirt, J. I. Clark, J. D. Wolchok, J. S. Weber, J. Tian, M. J. Yellin, G. M. Nichol, A. Hoos, W. J. Urba, *N. Eng. J. Med.* **2010**, *363*, 13.

[7] J. Brahmer, K. L. Reckamp, P. Baas, L. Crino, W. E. Eberhardt, E. Poddubskaya, S. Antonia, A. Pluzanski, E. E. Vokes, E. Holgado, D. Waterhouse, N. Ready, J. Gainor, O. Aren Frontera, L. Havel, M. Steins, M. C. Garassino, J. G. Aerts, M. Domine, L. Paz-Ares, M. Reck, C. Baudelet, C. T. Harbison, B. Lestini, D. R. Spigel, *N. Eng. J. Med.* **2015**, *373*, 2.

[8] A. M. Eggermont, V. Chiarion-Sileni, J. J. Grob, R. Dummer, J. D. Wolchok, H. Schmidt, O. Hamid, C. Robert, P. A. Ascierto, J. M. Richards, C. Lebbe, V. Ferraresi, M. Smylie, J. S. Weber, M. Maio, C. Konto, A. Hoos, V. de Pril, R. K. Gurunath, G. de Schaetzen, S. Suciu, A. Testori, *Lancet Oncol.* **2015**, *16*, 5.

[9] J. Larkin, V. Chiarion-Sileni, R. Gonzalez, J. J. Grob, C. L. Cowey, C. D. Lao, D. Schadendorf, R. Dummer, M. Smylie, P. Rutkowski, P. F. Ferrucci, A. Hill, J. Wagstaff, M. S. Carlino, J. B. Haanen, M. Maio, I. Marquez-Rodas, G. A. McArthur, P. A. Ascierto, G. V. Long, M. K. Callahan, M. A. Postow, K. Grossmann, M. Sznol, B. Dreno, L. Bastholt, A. Yang, L. M. Rollin, C. Horak, F. S. Hodi, J. D. Wolchok, *N. Eng. J. Med.* **2015**, *373*, 1.

[10] B. Weide, A. Martens, J. C. Hassel, C. Berking, M. A. Postow, K. Bisschop, E. Simeone, J. Mangana, B. Schilling, A. M. Di Giacomo, N. Brenner, K. Kahler, L. Heinzerling, R. Gutzmer, A. Bender, C. Gebhardt, E. Romano, F. Meier, P. Martus, M. Maio, C. Blank, D. Schadendorf, R. Dummer, P. A. Ascierto, G. Hospers, C. Garbe, J. D. Wolchok, *Clin. Cancer Res.* **2016**, *22*, 22.

[11] P. C. Tumeh, C. L. Harview, J. H. Yearley, I. P. Shintaku, E. J. Taylor, L. Robert, B. Chmielowski, M. Spasic, G. Henry, V. Ciobanu, A. N. West, M. Carmona, C. Kivork, E. Seja, G. Cherry, A. J. Gutierrez, T. R. Grogan, C. Mateus, G. Tomasic, J. A. Glaspy, R. O. Emerson, H. Robins, R. H. Pierce, D. A. Elashoff, C. Robert, A. Ribas, *Nature* **2014**, *515*, 7528.

[12] E. M. Van Allen, D. Miao, B. Schilling, S. A. Shukla, C. Blank, L. Zimmer, A. Sucker, U. Hillen, M. H. Foppen, S. M. Goldinger, J. Utikal, J. C. Hassel, B. Weide, K. C. Kaehler, C. Loquai, P. Mohr, R. Gutzmer, R. Dummer, S. Gabriel, C. J. Wu, D. Schadendorf, L. A. Garraway, *Science* **2015**, *350*, 6283.

[13] L. Carbognin, S. Pilotto, M. Milella, V. Vaccaro, M. Brunelli, A. Calio, F. Cuppone, I. Sperduti, D. Giannarelli, M. Chilosi, V. Bronte, A. Scarpa, E. Bria, G. Tortora, *PLoS One* **2015**, *10*, 6.

[14] P. Schmid, S. Adams, H. S. Rugo, A. Schneeweiss, C. H. Barrios, H. Iwata, V. Dieras, R. Hegg, S. A. Im, G. Shaw Wright, V. Henschel, L. Molinero, S. Y. Chui, R. Funke, A. Husain, E. P. Winer, S. Loi, L. A. Emens, *N. Eng. J. Med.* **2018**, *379*, 22.

[15] D. Schadendorf, D. E. Fisher, C. Garbe, J. E. Gershenwald, J. J. Grob, A. Halpern, M. Herlyn, M. A. Marchetti, G. McArthur, A. Ribas, A. Roesch, A. Hauschild, *Nat. Rev. Dis. Primers* **2015**, *1*, 15003.

[16] J. A. Webb, Y.-C. Ou, S. Faley, E. P. Paul, J. P. Hittinger, C. C. Cutright, E. C. Lin, L. M. Bellan, R. Bardhan, *ACS Omega* **2017**, *2*, 3583.

[17] S. Schlücker, *Angew. Chem. Int. Edit.* **2014**, *53*, 19.

[18] S. Schlücker, *ChemPhysChem* **2009**, *10*, 9.

[19] S. Schlücker, B. Küstner, A. Punge, R. Bonfig, A. Marx, P. Ströbel, *J. Raman Spectrosc.* **2006**, *37*, 7.

[20] M. Schütz, S. Schlücker, *PCCP* **2015**, *17*, 37.

[21] Y. Wang, S. Schlücker, *Analyst* **2013**, *138*, 8.

[22] M. Salehi, D. Steinigeweg, P. Ströbel, A. Marx, J. Packeisen, S. Schlücker, *J. Biophotonics* **2013**, *6*, 10.

[23] X.-P. Wang, Y. Zhang, M. König, E. Papadopoulou, B. Walkenfort, S. Kasimir-Bauer, A. Bankfalvi, S. Schlücker, *Analyst* **2016**, *141*, 17.

[24] X.-P. Wang, B. Walkenfort, M. König, L. König, S. Kasimir-Bauer, S. Schlücker, *Faraday Discuss.* **2017**, *205*, 377.

[25] Y. Zhang, S. Schlücker, in *Confocal Raman Microscopy*, Vol. 2 (Eds: J. Toporski, T. Dieing, O. Hollricher), Springer International Publishing, Basel, Switzerland **2018**.

[26] J. H. Yoon, F. Selbach, L. Langolf, S. Schlücker, *Small* **2018**, *14*, 4.

[27] Q. Ruan, L. Shao, Y. Shu, J. Wang, H. Wu, *Adv. Opt. Mater.* **2014**, *2*, 1.

[28] V. Tran, B. Walkenfort, M. König, M. Salehi, S. Schlücker, *Angew. Chem. Int. Edit.* **2019**, *58*, 2.

[29] P. H. C. Eilers, H. F. M. Boelens, Baseline Correction with Asymmetric Least Squares Smoothing, https://zanran_storage.s3.amazonaws.com/www.science.uva.nl/ContentPages/443199618.pdf (accessed: June 2019).

[30] J. H. Yoon, J. Lim, S. Yoon, *ACS Nano* **2012**, *6*, 8.

[31] N. J. Halas, S. Lal, W.-S. Chang, S. Link, P. Nordlander, *Chem. Rev.* **2011**, *111*, 6.

[32] J. Wissler, M. Wehmeyer, S. Bäcker, S. Knauer, S. Schlücker, *Anal. Chem.* **2018**, *90*, 1.

[33] V. Tran, C. Thiel, J. T. Svejda, M. Jalali, B. Walkenfort, D. Erni, S. Schlücker, *Nanoscale* **2018**, *10*, 46.

[34] I. Grenga, R. N. Donahue, L. Lepone, J. Bame, J. Schlom, B. Farsaci, *J. Immunother. Cancer* **2014**, *2*(Suppl 3), P102.

[35] Y. Zhang, X.-P. Wang, S. Perner, A. Bankfalvi, S. Schlücker, *Anal. Chem.* **2018**, *90*, 1.

SUPPORTING INFORMATION

Additional supporting information may be found online in the Supporting Information section at the end of this article.